Redox Biology 30 (2020) 101427

Contents lists available at ScienceDirect

Redox Biology

journal homepage: www.elsevier.com/locate/redox

Pro-survival and anti-inflammatory roles of NF-κB c-Rel in the Parkinson's disease models

Zishan Wang[a,1], Hongtian Dong[a,1], Jinghui Wang[a,1], Yulu Huang[a,1], Xiaoshuang Zhang[a], Yilin Tang[b], Qing Li[a], Zhaolin Liu[a], Yuanyuan Ma[a], Jiabin Tong[a], Li Huang[a], Jian Fei[c,d,e], Mei Yu[a,***], Jian Wang[a,b,**], Fang Huang[a,*]

[a] Department of Translational Neuroscience, Jing' an District Centre Hospital of Shanghai, State Key Laboratory of Medical Neurobiology and MOE Frontiers Center for Brain Science, Institutes of Brain Science, Fudan University, 138 Yixueyuan Road, Shanghai, 200032, China
[b] Department of Neurology, Huashan Hospital, Fudan University, 12 Wulumuqi Zhong Road, Shanghai, 200040, China
[c] School of Life Science and Technology, Tongji University, 1239 Siping Road, Shanghai, 200092, China
[d] Shanghai Research Center for Model Organisms, Pudong, Shanghai, 201203, China
[e] Shanghai Engineering Research Center for Model Organisms, Shanghai Model Organisms Center, INC., Shanghai, 201203, China

ARTICLE INFO

Keywords:
Parkinson's disease
NF-κB/c-Rel
Dopaminergic neurons
Microglia
Neuroprotection
Inflammation

ABSTRACT

The pathological hallmarks of Parkinson's disease (PD) are the progressive loss of dopaminergic (DA) neurons in the substantia nigra pars compacta (SNpc) and the presence of overactivated glial cells and neuroinflammation. Nuclear factor kappa-light-chain-enhancer of activated B cells (NF-κB) c-Rel subunit is closely related in the pathological progress of PD, however the roles and mechanisms of c-Rel in PD development remain unclear. Here, in neurotoxins-induced PD models, the dynamic changes of NF-κB c-Rel and its functions were evaluated. We found that c-Rel was rapidly activated in the nigrostriatal pathway, which mainly occurred in dopaminergic neurons and microglia. c-Rel could maintain neuronal survival by initiating the anti-apoptotic gene expression in MPP^+-treated SH-SY5Y cells and it could inhibit microglial overactivation by suppressing the inflammatory gene expression in LPS-challenged BV2 cells. c-Rel inhibitor IT901 aggravated the damage of MPTP on dopaminergic neurons and promoted the activation of microglia in the nigrostriatal pathway of mice. Moreover, the expression of c-Rel in blood samples of PD patients decreased dramatically. Our results indicate that the NF-κB/c-Rel subunit plays an important role in neuroprotection and neuroinflammation inhibition during PD progression.

1. Introduction

Parkinson's disease (PD) is the second most common neurodegenerative disease, which is characterized by the preferential loss of dopaminergic neurons in the substantia nigra pars compacta (SNpc) [1]. Growing evidence from studies in human PD brains, as well as in genetic and neurotoxin-induced animal PD models, indicates that neuroinflammation is a lasting feature of the disease and contributes to neurodegeneration [2,3]. The master transcription factor nuclear factor "kappa-light-chain-enhancer" of activated B-cells (NF-κB) regulates apoptosis/survival and inflammation in many types of cells [4,5]. The NF-κB family of transcription factors consists of five Rel-homology-containing proteins (c-Rel, Rel-A, Rel-B, NF-κB1 and NF-κB2) that form numerous homo- and heterodimers, which are normally retained in the cytoplasm through binding to inhibitors of NF-κB (IκB). NF-κB transcription factors are abundant in the brain and exhibit diverse functions [6]. Members of NF-κB family exist in neurons and glial cells in where they profoundly regulate expression of target gens, and contribute to both acute brain injury and neurodegenerative diseases [7–9]. Rel-A expression increases in the brains of MPTP-injured mice [10] and in the brain of PD subjects as well [11]. Various evidence shows that Rel-A activation is involved in neuronal loss and neuroinflammatory response

* Corresponding author. State Key Laboratory of Medical Neurobiology, Shanghai Medical College, Fudan University, 138 Yixueyuan Road, Shanghai, 200032, China.
** Corresponding author. Department of Neurology, Huashan Hospital, Fudan University. 12 Wulumuqi Zhong Road, Shanghai, 200040, China.
*** Corresponding author. State Key Laboratory of Medical Neurobiology, Shanghai Medical College, Fudan University, 138 Yixueyuan Road, Shanghai, 200032, China.
E-mail addresses: yumei@fudan.edu.cn (M. Yu), wangjian336@hotmail.com (J. Wang), huangf@shmu.edu.cn (F. Huang).
[1] These authors contributed equally to this work.

https://doi.org/10.1016/j.redox.2020.101427
Received 29 September 2019; Received in revised form 8 January 2020; Accepted 8 January 2020
Available online 13 January 2020

associated with PD progression [5,10]. However, the roles and mechanisms of c-Rel in PD remain to be elusive. Baiguera et al. found old c-Rel deficient mice develop a spontaneous late-onset PD-like phenotype [12], and there is a mild inflammatory profile without obvious signs of gliosis in *c-Rel*$^{-/-}$ mice [13]. In this study, the dynamic changes of NF-κB c-Rel subunit in the nigrostriatal pathway and its functions in PD were investigated in neurotoxins-induced PD models.

2. Materials and methods

2.1. Mice and PD model

12 to 14-week-old male C57BL/6 and NF-κB/c-Rel reporter mice [B6-Tg(c-Rel-luc)^{Mlit}] were obtained from Shanghai Model Organisms Center, INC. and housed under 12 h light/dark cycle with free access to food and water. Mice were injected intraperitoneally (i.p.) with MPTP-HCl (Sigma, USA) in 0.9% NaCl, using an acute dosing regimen of 20 mg/kg or 14 mg/kg (dose for detecting the in vivo effect of c-Rel inhibitor IT901) every 2 h for four doses. IT901 (Tocris, USA) was dissolved in DMSO at a stock concentration of 34 mg/ml and diluted with corn oil (the final concentration of DMSO was 5% (v/v)). IT901 (12 mg/kg) and vehicle (5% (v/v) DMSO in corn oil) was used for i.p. injection. All experimental protocols were approved by the Institutional Animal Care and Use Committee of Fudan University, Shanghai Medical College. All surgeries were performed under general anesthesia, and all efforts were made to minimize adverse effects.

2.2. Subjects

Sixteen patients with PD and nine healthy subjects were recruited from the Department of Neurology, Huashan Hospital, Fudan University. PD subjects were clinically examined and diagnosed by two senior investigators of movement disorders according to the UK Brain Bank criteria. All participants provided written informed consent in accordance with the Declaration of Helsinki. The study was approved by the Human Studies Institutional Review Board, Huashan Hospital, Fudan University. All methods were performed in accordance with the relevant guidelines and regulations. The demographic and clinical data of patients and controls are summarized in Supplementary Table 1.

2.3. In vivo imaging of luciferase activity

In vivo imaging was performed using an IVIS® Lumina III lumazone imaging system (PerkinElmer, USA). Mice were shaved and injected intraperitoneally with 150 mg/kg luciferin (dissolved in PBS, pH7.4) 45min after MPTP injection. 12 min later, mice were anesthetized with the mixture of isoflurane/oxygen and then placed on the imaging stage. Image was captured in completely darkness for 1 min. Photons emitted from specific regions were collected by the Lumazone and were quantified using Living imaging 4.5.5 software. The luciferase activity was presented in photon intensity per area.

2.4. Western blot

Proteins from tissues or cells were separated by SDS-PAGE and transferred to polyvinylidene fluoride (PVDF) membrane. Membrane was subsequently incubated with primary antibodies: Rabbit anti-Bcl-2 (1:500; Cell Signal Technology, USA), Rabbit anti-Bcl-xl (1:500; Abways, China), mouse anti-TH (1:2000; Sigma, USA), Rabbit anti-GFAP (1:2000; Dako, Japan), Rabbit anti-iNOS (1:500; Abcam, USA), Rabbit anti-COX2 (1:1000; Abcam, USA), Rabbit anti-IL-1β (1:1000; Santa Cruz, USA), Rabbit anti-Bax (1:1000; Cell Signal Technology, USA), Rabbit anti-SOD2 (1:1000; Abcam, USA), Rabbit anti-*c*-Rel (1:250; Santa Cruz, USA), Rabbit anti-H3 (1:1000; Cell Signal Technology, USA) and mouse anti-β-actin (1:2000; Santa Cruz, USA). Protein bands were detected and imaged using an Odyssey infrared imaging system (Li-Cor, USA). Densities were quantified using Quantity One 4.5.2 software (Bio-Rad, Hercules, USA).

2.5. Immunohistochemistry and immunofluorescence staining

For immunohistochemistry staining, brain slices (30 μm) were permeabilized, quenched the endogenous peroxidases with 0.3% H_2O_2. Slices were blocked in PBS containing 0.2% Triton X-100 and 10% normal goat serum at 37 °C for 45 min. Then slices were incubated with rabbit anti- Iba1 (1:1000; Wako, Japan) and mouse anti-TH (1:1000; Sigma, USA) in PBS with 1% goat serum at 4 °C overnight. After washing, the slices were incubated with biotinylated anti-rabbit or anti-mouse secondary antibodies (1:200; Vector Laboratories, USA) at 37 °C for 45 min and then with AB peroxidase (1:200; Vector Laboratories, USA) at 37 °C for 45 min. The peroxidase reaction was detected with Vectorlabs DAB Substrate Kit (Vector, USA).

For immunofluorescence staining, after being blocked in phosphate-buffered saline (PBS) containing 0.2% Triton X-100 and 10% normal goat serum at 37 °C for 45 min, brain slices were incubated at 4 °C for 48 h with antibodies: mouse anti-TH (1:500; Sigma, USA), rabbit anti-Iba1 (1:500; Wako, Japan), rabbit anti-GFAP (1:1000; Millipore, USA), mouse anti-*c*-Rel and rabbit anti-*c*-Rel (1:200, Santa Cruz, USA). After washing, the slices were incubated with secondary antibodies: Alexa Fluor 594-conjugated goat anti-mouse IgG and Alexa Fluor 488-conjugated goat anti-rabbit IgG (1:1000, ThermoFisher SCIENTIFIC, USA). Slices were coverslipped, and images taken under a Nikon confocal microscope (Nikon, Japan).

2.6. Quantification of Iba1$^+$ and TH$^+$ cells

Quantification of Iba1$^+$ cells in dorsal striatum was carried out according to our previous study [14] and analyzed with Image-Pro Plus 6.0 (Media Cybernetics, USA).

Total number of TH$^+$ neurons in the SNpc was quantified using a Stereo Investigator system (Micro Brightfield, USA), as described previously [14]. Stereological counting of microglia in the SNpc was carried out on midbrain sections using a rabbit anti-Iba1 antibody (1:1000; Wako, Japan). Mouse anti-TH antibody (1:500; Sigma, USA) was used to identify the SNpc as described by Martin et al. [15]. Staining was visualized using dye-conjugated secondary antibodies as in the method of immunofluorescence staining. Iba1$^+$ cells were counted using a fluorescence microscopy (Olympus, Japan) and the Stereo Investigator system (Micro Brightfield, USA). The experiment was performed in a double-blind fashion.

2.7. Cell culture and treatment

Human neuroblastoma cell line (SH-SY5Y) and mouse microglial BV2 cells were cultured in DMEM medium (Life technologies, USA) containing 300 mg/L glutamine, 10% FBS (fetal bovine serum), 1% Penicillin Streptomycin and kept at 37 °C in a humidified 5% CO2 incubator. SH-SY5Y and BV2 cells were grown on coverslips in 24-well plates at a density of 50,000 cells/well and 100,000 cells/well respectively. 24 h later, SH-SY5Y and BV2 cells with or without a 15 min' pretreatment of IT901 (2.5 μM) or vehicle (0.1% DMSO) were challenged with MPP$^+$ (1 mM) and LPS (100 ng/ml) respectively for different time.

2.8. Immunocytochemistry

Cells were fixed in 4% paraformaldehyde for 10 min and washed with PBS, and then permeabilized for 10 min in PBS containing 0.1% Triton X-100 (PBS-T) and blocked with 10% normal goat serum (Vector Laboratories, USA) in PBS. Then, cells were incubated with mouse anti-*c*-Rel and rabbit anti-*c*-Rel (1:200, Santa Cruz, USA) overnight at 4 °C. After washing, cells were incubated with Alexa Fluor 594-conjugated goat anti-mouse IgG and Alexa Fluor 488-conjugated goat anti-rabbit

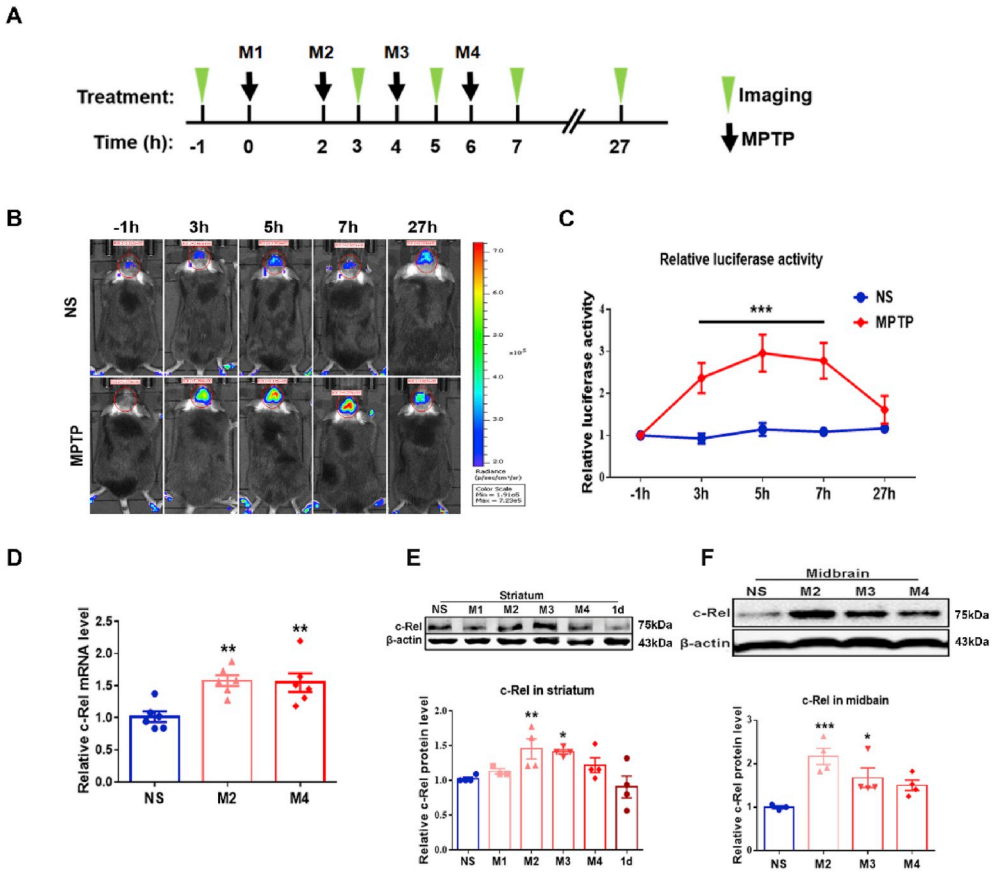

Fig. 1. The expression of c-Rel in the nigrostriatal pathway of MPTP-induced PD mice. (A) Experimental schedule. Luciferin was injected intraperitoneally 15 min ahead of imaging. **(B)** Representative images were depicted at the time points of −1, 3, 5, 7 and 27 h. The color scale was shown at the right. **(C)** Relative luciferase activities. n = 5–8 for the time point of 27 h; n = 8–12 for all the other time points. Differences were analyzed by two-way ANOVA followed by LSD multiple comparison tests. ***$p < 0.001$. **(D)** c-Rel transcripts in the striatum of mice treated with normal saline and 2 or 4 injections of MPTP. n = 6. **(E)** Western blot analysis of striatal c-Rel proteins. Quantification of relative c-Rel expression is shown at the bottom. n = 3–4. **(F)** Western blot analysis of c-Rel proteins in midbrain. Quantification of relative c-Rel expression is shown at the bottom. n = 3–4. NS: group of mice injected with normal saline; M1, M2, M3, M4: groups of mice challenged with one time, two times, three times, or four times i.p. injection of MPTP; 1d: group of mice challenged with four times i.p. injection of MPTP and samples were collected 1 day later. Differences were analyzed by one-way ANOVA followed by LSD multiple comparison tests.*$p < 0.05$, **$p < 0.01$, and ***$p < 0.001$, vs saline-treated control. (For interpretation of the references to color in this figure legend, the reader is referred to the Web version of this article.)

IgG (1:1000, ThermoFisher SCIENTIFIC, USA) for 1 h at room temperature. The coverslips were mounted, sealed. Images were taken by a confocal microscope (Nikon, Japan) at the same setting. For quantification, five fields were captured in a culture for counting cell numbers or measuring fluorescence brightness. Each field covers 50 to 150 cells.

2.9. Plasmid transfection

Sequences for c-Rel shRNA were as follows: human: 5′-GTTCGGTTG TTGTCTGTGCTGTGTTTTGGCCACTGACTGACACAGCACACAACAACC GAA-3’; mouse: 5′-GAACAATGGGAGGCAGAGCAGTGTTTTGGCCACTG ACTGA CACTGCTCTCTCCCATTGTT -3’. They were cloned into plasmid vector pcDNA3.1(+). The c-Rel overexpression plasmid was purchased from Addgene (USA). Cells were transfected with plasmids using lipofectamine 3000 (Invitrogen, USA). Transduced cell populations were selected 14 days after transfection using 900 μg/ml (SH-SY5Y cells) or 600 μg/ml (BV2 cells) G418 (Sigma-Aldrich, USA).

2.10. Cell proliferation assay

Cell proliferation was determined using Cell Counting Kit-8 (Beyotime, China) according to the manufacturer's instructions. Briefly, cells at 1×10^4 cells/well were seeded in a 96-well flat-bottomed plate, and grew at 37 °C for 24 h. Then medium was changed with 100 μl DMEM containing 1 mM MPP^+ or PBS. After 24 h, 10 μl CCK-8 was added to each well and the plate was incubated in a CO_2 incubator. The absorbance was determined at a wavelength of 450 nm using a microplate reader (Bio-Tech, USA).

2.11. Reactive oxygen species (ROS) analysis

After incubation with 1 mM MPP^+ or PBS for 24 h, cells were washed and incubated with 10 μM dihydroethidium (DHE) (Sigma, USA) at 37 °C for 30 min. Cells were then washed three times with PBS. Images were captured with Nikon fluorescence microscope and the fluorescence intensity was quantified by Image Pro Plus 6.0 (Media Cybernetics, USA).

2.12. LDH analysis

Cell death was assessed based on the amount of lactate hydrogenase (LDH) with a LDH Release Assay Kit (Beyotime, China). Briefly, SH-SY5Y cells were seeded in a 96-well flat-bottomed plate at a density of 10,000 cells/well, and grown at 37 °C for 24 h. 150 μl of fresh DMEM containing 1 mM MPP^+ or PBS was added. After 24 h, the plate was centrifuged for 5 min at 500 g in a centrifuge (Eppendorf, Germany) and 120 μl of supernatant was transferred to a new 96-well plate. 60 μl of working solution was added to each well and incubated for 30 min at room temperature. The absorbance was determined at a wavelength of 490 nm using a microplate reader (Bio-Tech, USA). The calculation formula is: Cytotoxicity (%) = OD490 (Experimental group - Control group)/OD490 (Positive control group - Control group) x 100.

2.13. Quantitative RT-PCR (qPCR)

Total RNA from cells was isolated using TRNzol (Tiangen, China). Total RNA from whole blood was extracted using HiPure Blood/Liquid RNA Kit (Magen, USA). Reverse transcription was carried out using random primer and Fastking gDNA dispelling RT SuperMix (Tiangen, China). Quantitative PCR was performed using a SuperReal PreMix Plus (SYBR Green) (Tiangen, China). The relative expression value of the target gene was calculated as the ratio of target cDNA to β-actin. The primers used in the real-time PCR were listed in Supplementary Table 2.

2.14. Statistical analysis

Data are expressed as the means ± SEM. Data were assessed for normal distribution by Shapiro-Wilk test. For two group comparisons, two-tailed unpaired Student's t-test or Mann-Whitney test was used as appropriate. For more than two group comparisons, one-way ANOVA followed by LSD multiple comparison tests or Kruskal-Wallis test followed by Dunn's multiple comparison tests were used as appropriate. A two-way ANOVA followed by a LSD multiple comparison test was conducted for the relative luciferase activities in Fig. 1C. In in vitro experiments, the value "n" represents independent biological repeats. Statistical analysis was performed with PRISM 7.0 (GraphPad Software Inc, USA). Statistically significant differences were defined as $p < 0.05$.

3. Results

3.1. Dynamic changes of c-Rel expression in the nigrostriatal pathway of MPTP-induced PD mice

NF-κB/c-Rel reporter mouse B6-Tg(c-Rel-luc)^{Mlit} [16] was used to monitor c-Rel expression in MPTP-induced model of PD. The experimental schedule was shown in Fig. 1A. The expression of luciferase increased dramatically at 1 h after the second injection of MPTP. The luminescent signals reached the peak value after the third and fourth injection, and gradually declined afterwards. The signals exhibited no difference between MPTP- and saline-treated groups at 27 h post injection. The time courses of luciferase activities after MPTP administration were present in Fig. 1B and C. The expression of c-Rel in the striatum and midbrain was assessed at both transcriptional and translational levels. One hour after the second and fourth injection of MPTP, c-Rel transcripts in striatum were markedly elevated (Fig. 1D). Two injections of MPTP resulted in increased c-Rel protein levels in both striatum and midbrain; however, c-Rel proteins were comparable between MPTP- and saline-treated groups after four injections of MPTP (Fig. 1E and F).

3.2. Nucleus translocation of c-Rel in dopaminergic neurons and microglia early after MPTP administration

Early events including loss of TH^+ fiber and glial activation were investigated. We found a rapid and apparent depletion of striatal TH^+ nerve terminals induced by three or four times MPTP exposure (Fig. 2A). Microglial cell numbers increased dramatically after the fourth MPTP injection in the striatum (Fig. 2B). In the substantia nigra (SN) of mice challenged with three injections of MPTP, $Iba1^+$ cell numbers did not alter (Supplementary Fig. S1A). The astrocytic activation was also evaluated. At early time points of M3 and M4, $GFAP^+$ astrocytes did not change in the nigrostriatal pathway (Supplementary Fig. S1B). The cell types in which c-Rel was expressed and activatable in the MPTP model of PD were illustrated by double immunostaining. Three times injection of MPTP stimulated c-Rel nuclear translocation in striatal microglial cells (Fig. 2C). As a control, brain sections stained without primary c-Rel antibody or secondary antibody were shown in Supplementary Fig. 2. The co-localization of c-Rel and DNA dye DAPI in TH^+ neurons after the third MPTP administration increased compared to the saline group (Fig. 2D). At 7 days after the treatment of MPTP, astrocytes in the substantia nigra were activated, however, nuclear translocation of c-Rel was rarely detected (Supplementary Fig. S3A). Additionally, in primary cultured astrocytes exposed to MPP^+ for 0, 0.5, 1.5, 3, 6–9 h, co-localization of c-Rel and DAPI showed no obvious difference (Supplementary Fig. S3B).

3.3. Pro-survival role of c-Rel in dopaminergic SH-SY5Y cells

MPP^+-intoxicated SH-SY5Y cells are commonly used as a cellular PD model. The c-Rel transcripts in SH-SY5Y cells treated with PBS or MPP+ were assessed by real-time PCR. We found c-Rel expression increased dramatically in cells with 9 h' treatment of MPP^+ and the elevated expression of c-Rel was sustained at 24 h after MPP^+ exposure (Fig. 3A). Using immunofluorescence staining and Western blot, we investigated the nuclear translocation of c-Rel in MPP^+-treated SH-SY5Y cells. c-Rel was mainly distributed in the cytoplasm compartment under normal culture conditions. MPP^+-treatment gradually induced the nuclear translocation of c-Rel. Nuclear signals of c-Rel and nuclear c-Rel protein levels reached peak at 3–6 h post treatment, and maintained significantly higher afterwards (Fig. 3B, Supplementary Fig. 4A). The percentage of cells with nuclear c-Rel showed parallel changes. Next, plasmids pcDNA3.1-hu c-Rel shRNA (shRNA) and pcDNA3.1-FLAG-hu c-Rel (OE) were used to knockdown or overexpress human c-Rel in SH-SY5Y cells respectively (Fig. 3C and D). c-Rel-modified and control SH-SY5Y cells were subjected to MPP^+ intoxication and cell viabilities were evaluated. There were no differences between cells of control and shRNA or OE treated with PBS, however, MPP^+ exposure caused more dramatic reduction in cell viability and higher LDH release in shRNA group compared to control cells (Fig. 3E, Supplementary Fig. S4B), whereas, cells in OE group showed higher cell viability than the control (Fig. 3E). The compound IT901 is a specific inhibitor of c-Rel. IT901 at concentrations higher than 2.5 μM had toxic effects in SH-SY5Ycells, and it could inhibit c-Rel activity in MPP^+-treated SH-SY5Y cells (Supplementary Figs. S4C–E). We found cells treated with 2.5 μM IT901 were more sensitive to the insult of MPP^+ (Fig. 3F).

MPP^+ treatment increased intracellular ROS levels in SH-SY5Y cells [17]. Using ROS probe DHE, we found there were no differences in ROS levels between cells of control and shRNA or OE treated with PBS, however, MPP^+ challenge markedly increased the production of ROS in SH-SY5Y cells. MPP^+ elicited more or less ROS products in c-Rel shRNA or c-Rel OE cells respectively (Fig. 4A). Pro-survival gene Bcl-xl and anti-oxidative gene SOD2 are c-Rel targets. By Western blot, we found that in c-Rel knockdown SH-SY5Y cells, MPP^+ treatment reduced Bcl-xl, SOD2 expression, and the ratio of Bcl-2 to Bax as well when compared to PBS-treated c-Rel shRNA cells and MPP^+-treated control cells (Fig. 4B). On the contrary, in c-Rel OE cells, transcripts of *Bcl-2*, *Bcl-xl* and *SOD2* increased significantly (Fig. 4C). Bcl-2 and Bcl-xl protein levels in c-Rel OE cells were markedly elevated compared to control cells (Fig. 4D). After MPP^+ treatment, expression of Bcl-2, Bcl-xl and SOD2 in c-Rel OE cells increased dramatically compared to MPP^+-treated control cells (Fig. 4D).

3.4. Anti-inflammatory role of c-Rel in BV2 microglial cells

In the SNpc of PD patients, activated microglia express and release inflammatory molecules like NO and Interleukin- 1β (IL-1β). Role of c-Rel in LPS-treated BV2 microglial cells was further investigated. Using qPCR, c-Rel expression in BV2 cells treated with LPS for 0, 2, 4, 6, 8, 12, and 24 h was assessed. An elevated expression of c-Rel was induced in BV2 cells with 2 h' LPS treatment, and c-Rel transcripts were down-regulated rapidly afterwards, and maintained the baseline expression at 6–24 h after LPS challenge (Fig. 5A). By immunofluorescence staining, we found c-Rel was mainly located in the cytoplasm of resting BV2 cells. LPS stimulation promoted c-Rel nuclear translocation. At the time point of 2 h, nuclear c-Rel signal reached the highest level (Fig. 5B). By Western blot, nuclear c-Rel proteins showed similar tendency (Fig. 5C). Next, plasmids pcDNA3.1-mu c-Rel shRNA (shRNA) and pcDNA3.1-FLAG-mu c-Rel (OE) were used to knockdown or overexpress mouse c-Rel in BV2 cells respectively (Fig. 5D and E). c-Rel-modified and control BV2 cells were subjected to LPS stimulation and medium NO_2^- levels were measured. There were no differences between cells of Control and shRNA or OE treated with PBS, however, LPS treatment resulted in more dramatic elevation in NO_2^- concentration in shRNA group compared to the control (Fig. 5F), whereas, NO_2^- production in OE group was significantly lower than that in the control cells (Fig. 5G). c-

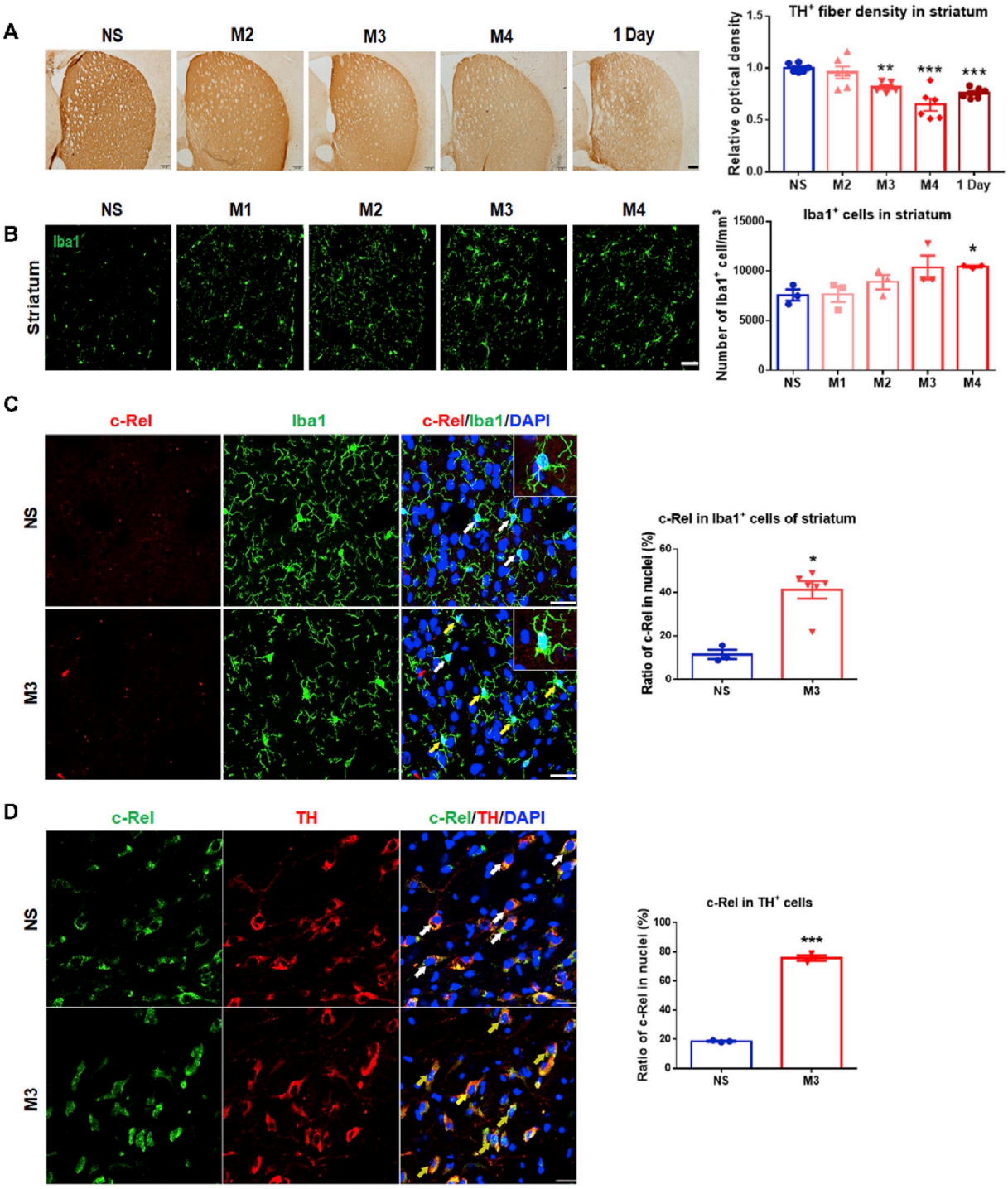

Fig. 2. Depletion of dopaminergic terminals, microglial activation and nuclear translocation of c-Rel in the nigrostriatal pathway of MPTP-induced PD mice. (A) Immunohistochemical staining of TH in the striatum. Scale bar: 200 μm. Densitometric analysis of TH staining is shown in the right panel. n = 5–6. Differences were analyzed by one-way ANOVA followed by LSD multiple comparison tests. $^{**}p < 0.01$, $^{***}p < 0.001$, vs saline-treated control. **(B)** Immunofluorescence staining of Iba1 in the striatum of mice treated with saline, one, two, three or four injections of MPTP. Scale bar: 50 μm. Quantification of $Iba1^+$ cells is shown in the right panel. n = 3. Differences were analyzed by Kruskal-Wallis test followed by Dunn's multiple comparison tests. $^{*}p < 0.05$, vs saline-treated control. **(C)** Immunofluorescence staining of c-Rel (red) and Iba1 (green) in the striatum, scale bar: 25 μm. White arrows indicate cells with c-Rel in the cytoplasm; Yellow arrows indicate cells with c-Rel in the nuclei. Quantification of $Iba1^+$ cells with c-Rel in the nuclei is shown in the right panel. Difference was analyzed by Mann Whitney test. $^{*}p < 0.05$. n = 3–5. **(D)** Immunofluorescence staining of c-Rel (green) and TH (red) in the SN, scale bar: 25 μm. White arrows indicate cells with c-Rel in the cytoplasm; Yellow arrows indicate cells with c-Rel in the nuclei. Quantification of TH^+ cells with c-Rel in the nuclei is shown in the right panel. Difference was analyzed by unpaired two-tailed Student's t-test. $^{***}p < 0.001$. n = 3–5. (For interpretation of the references to color in this figure legend, the reader is referred to the Web version of this article.)

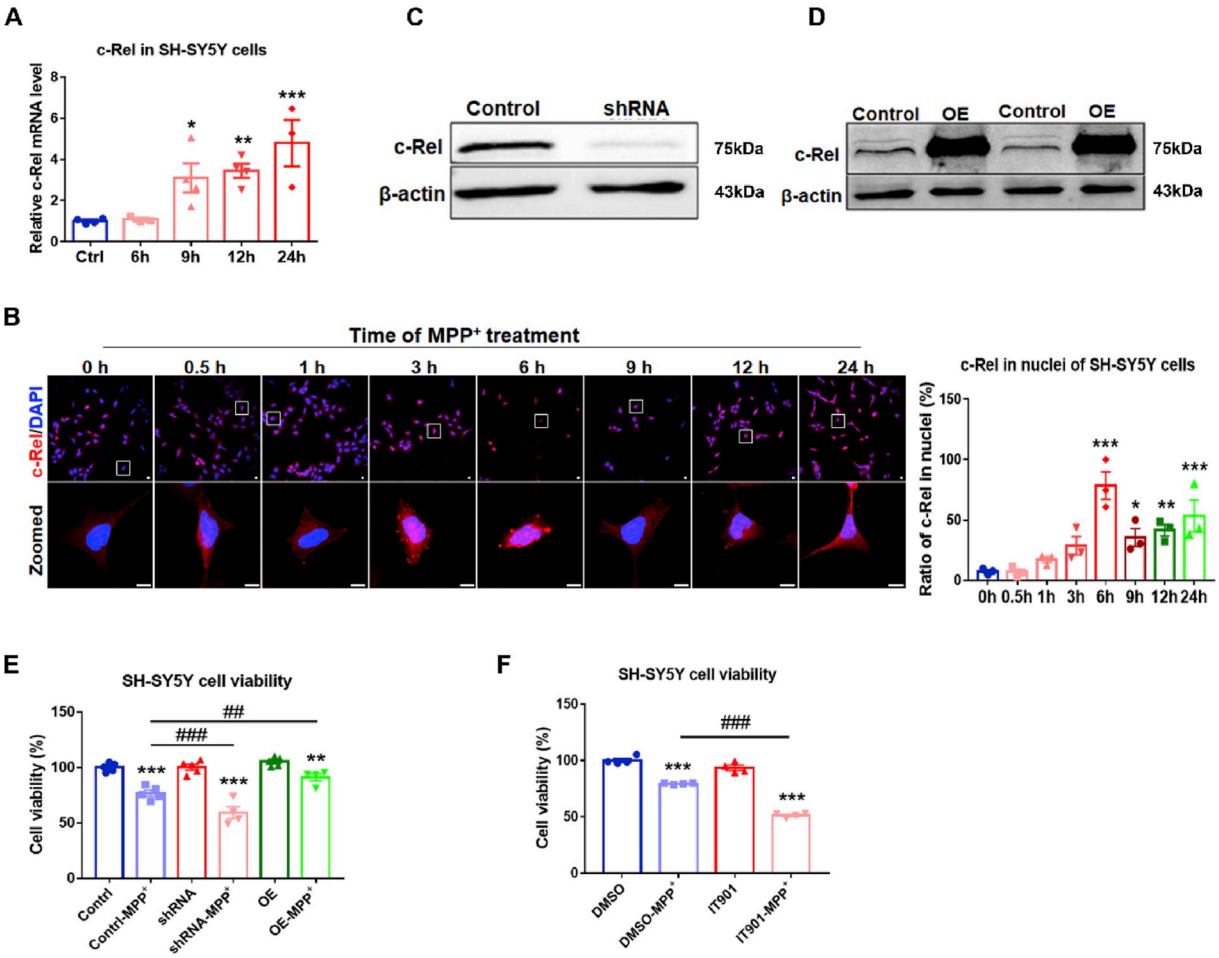

Fig. 3. Expression of c-Rel in SH-SY5Y cells and the effects of c-Rel on cell survival. (A) qPCR analysis of c-Rel transcripts in SH-SY5Y cells treated with MPP^+ for 6, 9, 12 and 24 h n = 3–4. **(B)** Immunofluorescence staining of c-Rel (red) in SH-SY5Y cells treated with MPP^+ for 0, 0.5, 1, 3, 6, 9, 12 and 24 h. Photos of high magnification are shown in lower panel. Scale bar: 10 μm. Quantification of cells with c-Rel in the nuclei is shown at the right. n = 3. **(C)** Downregulation of c-Rel expression in c-Rel shRNA SH-SY5Y cells. **(D)** Overexpression of c-Rel in c-Rel OE SH-SY5Y cells. **(E)** Cell viability assays in Control, c-Rel shRNA and c-Rel OE cells treated with MPP^+ or PBS for 24 h n = 4–5. **(F)** Effect of c-Rel inhibitor IT901 on cell viability. n = 4. Differences were analyzed by one-way ANOVA followed by LSD multiple comparison tests. $*p < 0.05$, $**p < 0.01$, $***p < 0.001$, vs control groups; $\#\#p < 0.01$, $\#\#\#p < 0.001$, *vs* MPP^+-treated control groups. (For interpretation of the references to color in this figure legend, the reader is referred to the Web version of this article.)

Rel inhibitor IT901 at a concentration higher than 5 μM caused toxicity to BV2 cells and IT901 at 2.5 μM could inhibit c-Rel activity in LPS-treated BV2 cells (Supplementary Fig. S5). We found BV2 cells treated with IT901 produced more NO compared to DMSO-treated cells after LPS stimulation (Fig. 5H).

Expression of pro-inflammatory molecules *IL-1β*, *TNF-α*, *IL-6*, and *iNOS* was tested by qPCR. All these four transcripts in control BV2 cells were upregulated by LPS stimulation, and were further elevated in c-Rel shRNA BV2 cells (Fig. 6A and B). Compound PDTC inhibits activation of NF-kB pathway. Treatment of PDTC reduced *iNOS* and *COX2* expression in both control and c-Rel knockdown BV2 cells stimulated with LPS (Fig. 6B, Supplementary Fig. S6). COX2, Bcl-xl, IL-1β, and iNOS proteins in control and c-Rel knockdown BV2 cells were determined by Western blot. We found that IL-1β protein level increased, whereas Bcl-xl decreased ($p = 0.022$ by unpaired *t*-test) in c-Rel knockdown BV2 cells compared to control BV2 cells. After LPS stimulation, COX2, iNOS and Bcl-xl protein levels were dramatically upregulated in both control and c-Rel shRNA BV2 cells, however, COX2 and iNOS proteins were further elevated in c-Rel shRNA BV2 cells (Fig. 6C). In c-Rel overexpression cells, transcripts of *IL-1β*, *TNF-α* and *iNOS* decreased compared to control BV2 cells (by unpaired *t*-test), whereas, *IL-6* did not alter between the two groups (Fig. 6D). After LPS treatment, transcripts of *IL-1β*, *TNF-α*, *IL-6*, and *iNOS* increased significantly in both control and c-Rel OE BV2 cells, however, *IL-1β*, *IL-6* and *iNOS* expression in c-Rel OE BV2 cells was dramatically lower compared to control BV2 cells (Fig. 6D), and iNOS and COX2 protein levels in c-Rel OE BV2 cells was significantly reduced as well (Fig. 6E). c-Rel inhibitor IT901 upregulated iNOS and COX2 expression in LPS-treated BV2 cell (Fig. 6F).

3.5. *Effects of c-Rel specific inhibitor IT901 in an MPTP-induced mouse model of PD*

The effects of c-Rel inhibitor on MPTP-injured nigrostriatal pathway were investigated including damages to the dopaminergic system and glial activation. Systemic administration of IT901 reduced c-Rel expression in c-Rel reporter mice [18]. Here, IT901 or vehicle was administered by intraperitoneal injection 45 min ahead of MPTP or normal saline administration. Mice were divided into 4 groups: Control, IT901, MPTP and IT901/MPTP. The experimental schedule was in Supplementary Fig. S7A. By immunohistochemical staining and stereological cell counting, and Western blot, we found the TH^+ cell numbers in the SNpc, and TH protein levels and TH^+ fiber densities in the striatum decreased significantly in mice challenged with MPTP, however the reductions were more severe in IT901-MPTP group (Fig. 7A, B, C).

Microglial activation was observed in the nigrostriatal pathway 2

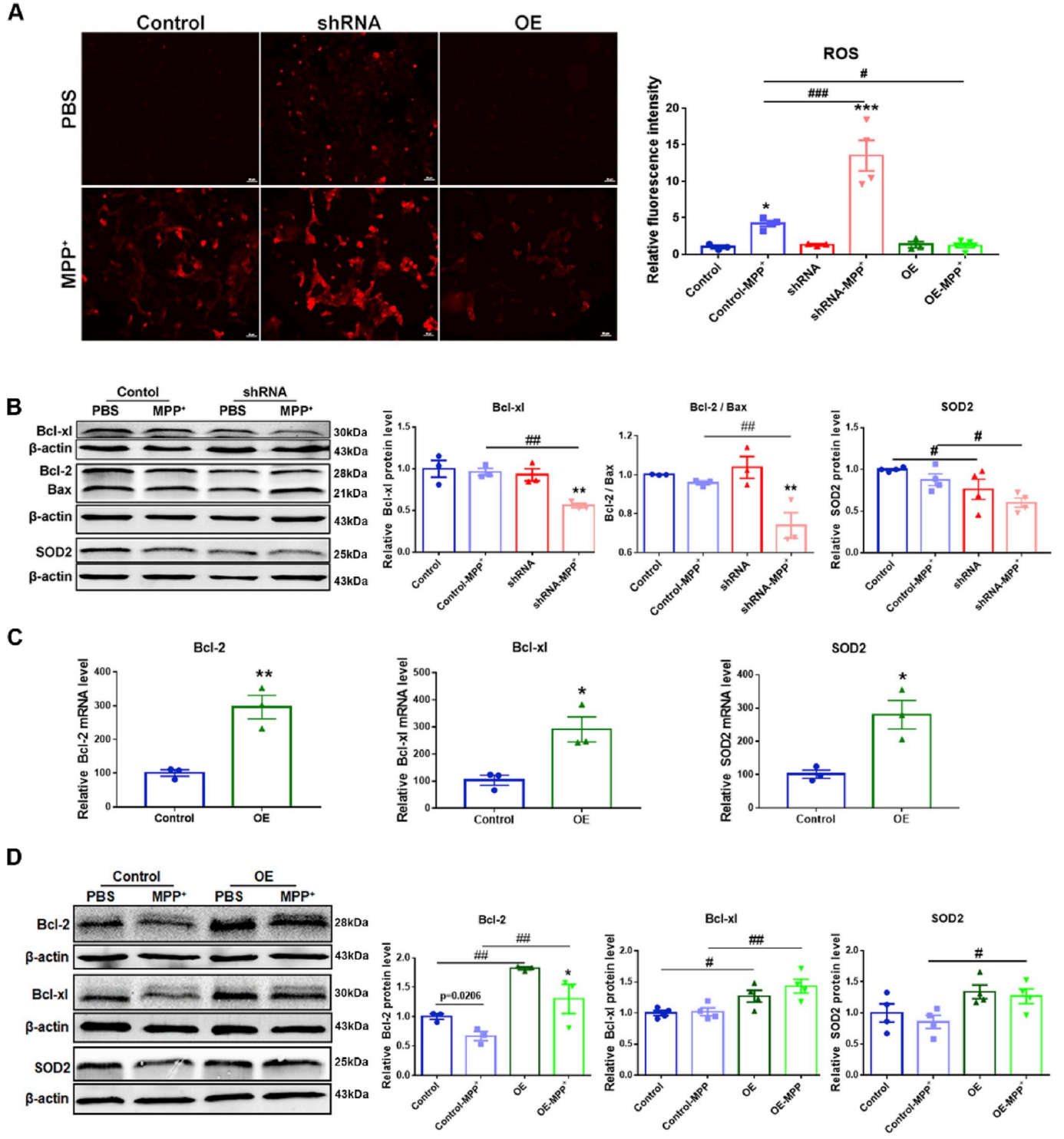

Fig. 4. Pro-survival pathways of c-Rel in SH-SY5Y cells. (A) Intracellular ROS indicated by DHE probe in Control, c-Rel shRNA, and c-Rel OE SH-SY5Y cells treated with MPP^+ or PBS for 24 h. Scale bar: 50 μm. Quantifications of intracellular ROS intensities are shown in the right panel. n = 3–5. Differences were analyzed by one-way ANOVA followed by LSD multiple comparison tests. $*p < 0.05$, vs PBS groups. **(B)** Western blot analysis of Bcl-xl, Bcl-2, Bax and SOD2 proteins in control and c-Rel knockdown SH-SY5Y cells. Quantifications of relative Bcl-xl, SOD2 expression and the ratio of Bcl-2 to Bax are shown in the right panel. n = 3. Differences were analyzed by one-way ANOVA followed by LSD multiple comparison tests. $**p < 0.01$, vs PBS group; $\#p < 0.05$, $\#\#p < 0.01$, vs groups of control. **(C)** Transcripts of *Bcl-2*, *Bcl-xl* and *SOD2* in control and c-Rel OE SH-SY5Y cells. n = 3. Differences were analyzed by unpaired two-tailed Student's t-test. **(D)** Western blot analysis of Bcl-2, Bcl-xl and SOD2 proteins in Control and c-Rel OE SH-SY5Y cells. Quantifications of relative Bcl-2, Bcl-xl and SOD2 expression are shown in the right panel. n = 3–4. Differences were analyzed by one-way ANOVA followed by LSD multiple comparison tests. $**p < 0.01$, vs PBS group; $\#p < 0.05$, $\#\#p < 0.01$, vs groups of control. P value in numbers was analyzed by unpaired two-tailed Student's t-test.

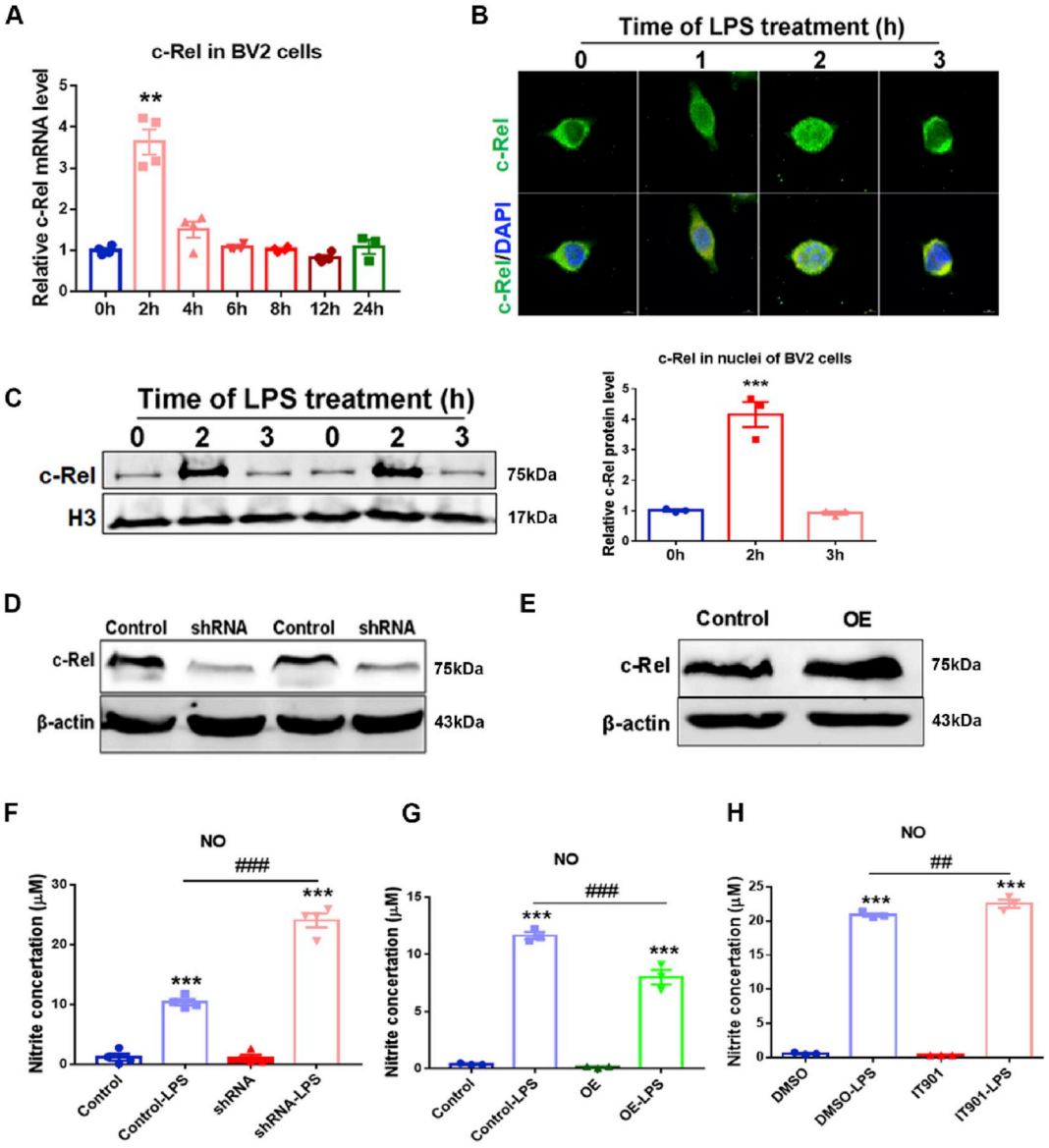

Fig. 5. Expression of c-Rel in BV2 cells and the effects of c-Rel on NO production. (A) qPCR analysis of c-Rel transcripts in BV2 cells treated with 100 ng/ml LPS for 2, 4, 6, 8, 12 and 24 h n = 4. Differences were analyzed by Kruskal-Wallis test followed by Dunn's multiple comparison tests. $^{**}p < 0.01$, vs control group. **(B)** Immunofluorescence staining of c-Rel (green) in BV2 cells treated with 100 ng/ml LPS for 0, 1, 2 and 3 h. Scale bar: 10 μm. **(C)** Western blot analysis of nuclear c-Rel proteins in BV2 cells treated with 100 ng/ml LPS for 0, 2 and 3 h. H3 protein served as a loading control. n = 3. Differences were analyzed by one-way ANOVA followed by LSD multiple comparison tests. $^{***}p < 0.001$, vs control group. **(D)** Downregulation of c-Rel expression in c-Rel shRNA BV2 cells. **(E)** Overexpression of c-Rel in c-Rel OE BV2 cells. **(F)** NO_2^- production assays in Control and c-Rel shRNA cells treated with 100 ng/ml LPS or PBS for 24 h n = 4. **(G)** NO_2^- production assays in Control and c-Rel OE BV2 cells treated with 100 ng/ml LPS or PBS for 24 h n = 4. **(H)** Effect of c-Rel inhibitor IT901 on NO_2^- production. n = 3. Differences were analyzed by one-way ANOVA followed by LSD multiple comparison tests. $^{***}p < 0.001$, vs PBS groups; $^{\#\#}p < 0.01$, $^{\#\#\#}p < 0.001$, vs LPS-treated control groups. (For interpretation of the references to color in this figure legend, the reader is referred to the Web version of this article.)

days after MPTP administration, which was indicated by increased $Iba1^+$ cell numbers and changes in morphology (Fig. 7D and E). In the SNpc, microglial cell number was further elevated in the group of IT901-MPTP compared to the group of DMSO-MPTP (Fig. 7D, Supplementary Fig. S7B), whereas in the striatum of IT901-MPTP mice, $Iba1^+$ cell number showed no alteration compared to DMSO-MPTP mice (Fig. 7E, Supplementary Fig. S7C). Pole test, rearing test and rotarod test were conducted to assess mouse behaviors. MPTP exposure impaired behaviors in mice, however, no differences regarding locomotor ability and motor coordination were detected between the groups of DMSO-MPTP and IT901-MPTP (Supplementary Figs. S7D–F).

3.6. The expression of NF-κB subunits in whole blood samples from PD patients and control subjects

The expression of NF-κB subunits Rel-A, c-Rel and NF-κB 1 in whole blood samples from PD patients and control subjects was measured by quantitative RT-PCR. The main demographic and clinical characteristics of the 35 idiopathic PD patients and 27 controls recruited in this study are summarized in Supplementary Table 1. We found that the transcript of *c-Rel* decreased, whereas the transcript of *NF-κB 1* increased and the transcript of *Rel-A* increased, but not significantly, in blood samples of PD patients. Notably, the ratios of c-Rel to Rel A and c-Rel to NF-κB 1 were markedly lower in PD blood samples compared to those of the controls. Additionally, the ratio of NF-κB 1 to Rel-A did not alter in the two groups (Fig. 7F). Moreover, the sensitivity and

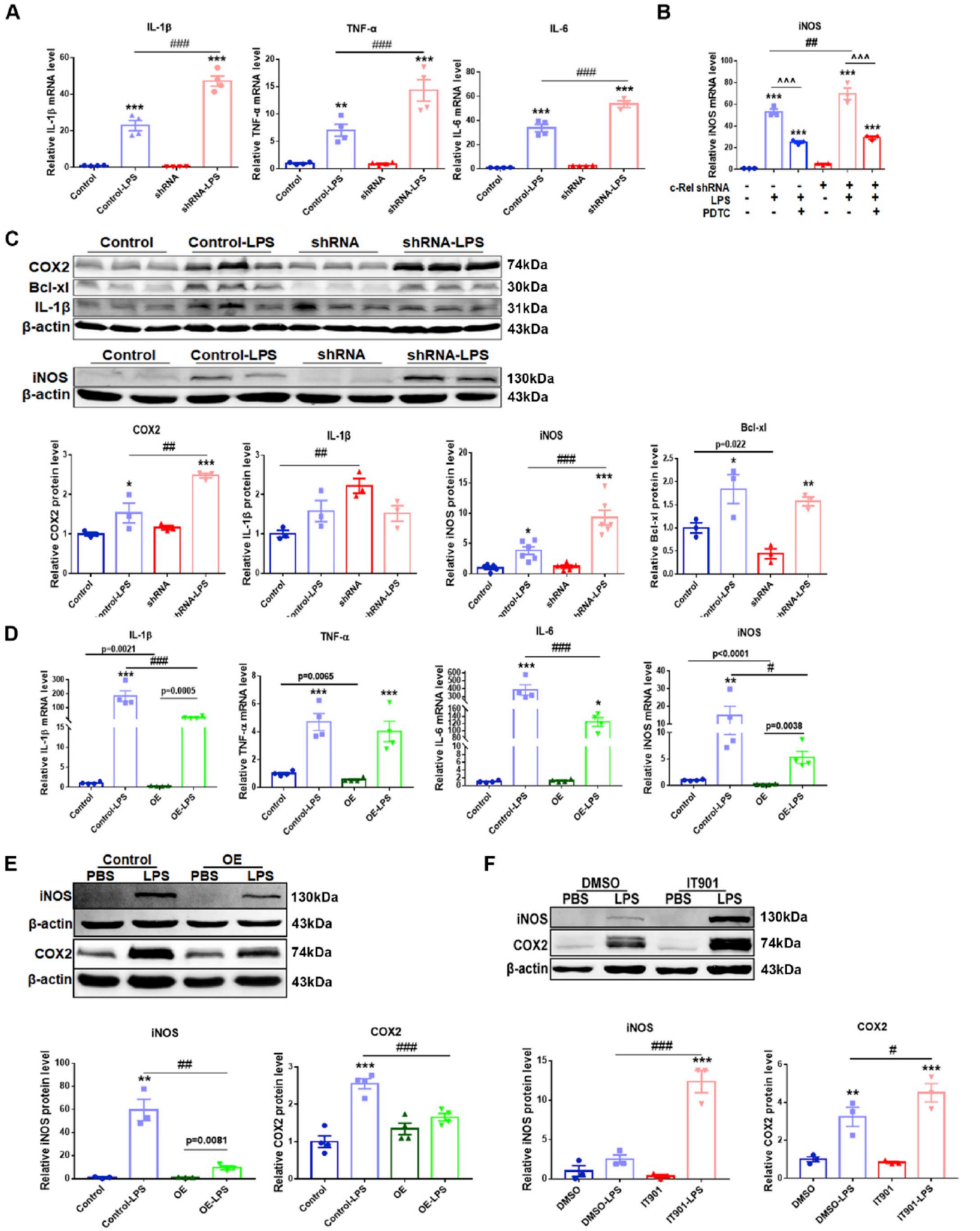

(caption on next page)

Fig. 6. Anti-inflammation pathways of c-Rel in BV2 cells. (A) Transcripts of *IL-1β*, *TNF-α*, *IL-6* and *iNOS* in Control and c-Rel shRNA BV2 cells treated with PBS or 100 ng/ml LPS for 6 h n = 4. Differences were analyzed by one-way ANOVA followed by LSD multiple comparison tests. $^{**}p < 0.01$, $^{***}p < 0.001$, vs PBS groups; $\#\#\#p < 0.001$, vs LPS-treated control groups; **(B)** Effect of PDTC on iNOS expression in BV2 cells. n = 3. Differences were analyzed by one-way ANOVA followed by LSD multiple comparison tests. $^{***}p < 0.001$, vs PBS groups; $\#\#p < 0.01$, vs LPS-treated control groups; $\hat{}\hat{}\hat{}p < 0.001$, vs LPS-treated groups. **(C)** Western blot analysis of COX2, Bcl-xl, IL-1β and iNOS proteins in control and c-Rel knockdown BV2 cells. Quantifications of relative COX2, Bcl-xl, IL-1β and iNOS are shown in the right and bottom panels. n = 3. **(D)** *IL-1β*, *TNF-α*, *IL-6* and *iNOS* transcripts in Control and c-Rel OE BV2 cells treated with PBS or 100 ng/ml LPS for 6 h n = 4. **(E)** Western blot analysis of iNOS and COX2 proteins in Control and c-Rel OE BV2 cells. Quantifications of relative iNOS and COX2 expression are shown in the right panel. n = 3–4. **(F)** Western blot analysis of iNOS and COX2 proteins in BV2 cells stimulated with PBS or 100 ng/ml LPS combined with DMSO or IT901 for 24 h. Quantifications of relative iNOS and COX2 expression are shown in the right panel. n = 3. Differences were analyzed by one-way ANOVA followed by LSD multiple comparison tests. $^{*}p < 0.05$, $^{**}p < 0.01$, $^{***}p < 0.001$, vs control groups; $\#p < 0.05$, $\#\#p < 0.01$, $\#\#\#p < 0.001$, *vs* LPS-treated control groups. P values in numbers were analyzed by unpaired two-tailed Student's t-test.

specificity of the results were evaluated by ROC analysis. As shown in Supplementary Fig. 7G, the index of c-Rel expression has the highest priority indicated by the area under curve (AUC).

4. Discussion

In this study, dynamic expression and activation of c-Rel were assessed in MPTP-intoxicated B6-Tg(c-Rel-luc)^{Mlit} NF-κB/c-Rel reporter mice and C57BL/6 mice, and neurotoxin-treated cellular PD models. MPTP administration induced rapid increases of c-Rel transcript and protein in the nigrostriatal pathway, and rapid nuclear translocations in dopaminergic neurons and microglial cells, but not in astrocytes. In MPP^+-induced cellular PD model, c-Rel expression was upregulated and its activation was persistent in SH-SY5Y cells. c-Rel knockdown and overexpression cells were more sensitive to and resistant to MPP^+ toxicity respectively. In LPS-stimulated BV2 cells, the changes in expression and activation of c-Rel were temporary. The peak values occurred at 2 h afterwards, and then went back sharply to the baseline. Expression of inflammatory molecules was enhanced and inhibited respectively in c-Rel knockdown and overexpression BV2 cells. On the contrary, c-Rel in astrocytes showed no remarkable alterations.

NF-κB transcription factors are the core factors dictating cell fate. Homeostasis of NF-κB members is critical for gene expression network in relation to apoptosis and inflammation. The activation of a distinct combination of NF-κB subunits may cause the differential regulation of target genes. Opposing effects of NF-κB/Rel-A and c-Rel subunits on neuronal survival have been demonstrated. Pizzi et al. found Rel-A is necessary for glutamate-induced cell death [19]. Various antioxidants exert neuroprotective effects through inhibiting the release of glutamate [20–22]. Downregulation of Rel-A levels by such antioxidants might be the underlying mechanism. Activation of Rel-A leads to IL-17-induced death of midbrain neurons [23]. On the contrary, c-Rel protects neurons against ranges of insults including Aβ intoxication and ischemia [24,25] and mediates pro-survival effects of interleukin-1β [19]. In the present study, we found while c-Rel knockdown induced intracellular ROS production and reduced the cell viability, c-Rel overexpression suppressed ROS generation and promoted the viability of SH-SY5Y cells exposed to MPP^+, which is in line with the general neuroprotection role of c-Rel.

In PD patients and PD animal model, Rel-A increased evidently both in dopaminergic neurons and glial cells in the substantia nigra area [10,11]. NF-κB members in glia show a low basal activity and are highly inducible, and they play a critical role in brain inflammation and neurodegeneration. However, role of c-Rel in glial activation in PD is quite unknown. A rapid c-Rel activation, as indicated by nuclear translocation, was detected both in microglial cells of MPTP-injured striatum, and LPS-stimulated BV2 cells. In c-Rel OE BV2 cells, c-Rel-containing dimmers might compete with Rel-A-containing dimmers and downregulate pro-inflammatory target genes, whereas in c-Rel shRNA BV2 cells, a defect of c-Rel activity might be associated with higher Rel-A activation and enhanced transcriptions of pro-inflammatory targets. This premise is supported in *c-Rel* deficient mice which develop a late-onset form of Parkinsonism due to higher Rel-A activity and reduction in SNpc resilience to aging [5,12]. PDTC is a relatively selective inhibitor of NF-κB activation [26]. iNOS expression in PDTC + LPS-treated c-Rel shRNA BV2 cells was comparable to PDTC + LPS-treated control BV2 cells, suggesting higher NF-κB activation mediated the hyper-transcriptions of inflammatory molecules in c-Rel knockdown cells.

In the SNpc of PD patients, loss of dopaminergic neurons is accompanied with microglial activation. c-Rel has pro-survival and anti-inflammation activities. We further analyzed the expression of apoptosis-related proteins Bcl-xl, Bcl-2 [27–29] and free radical scavenging protein SOD2 [30,31] in SH-SY5Y cells, and inflammation-related proteins COX-2, IL-1β and iNOS in BV2 cells. Higher protein levels of Bcl-xl, Bcl-2 and SOD2 detected in MPP^+-treated c-Rel OE SH-SY5Y cells contributed to increased cellular viability compared to MPP^+-treated control cells. Whereas, increased COX-2, IL-1β, iNOS proteins, and higher level of NO promoted the inflammatory activation of LPS-stimulated c-Rel knockdown BV2 cells.

As a specific inhibitor of NF-κB/c-Rel subunit, IT901 can effectively inhibit c-Rel activity and mediates anticancer properties in hematologic malignancies in mice, systemic administration of IT901 reduced c-Rel expression in brains of c-Rel reporter mice challenged with LPS [18]. Here, we found IT901 aggravated damages to the nigrostriatal dopaminergic system induced by MPTP, and IT901 exacerbated microglial activation in the SNpc, but not in striatum. In previous studies, we found the mode of activation and restoration of resting state of microglia in the striatum was faster than in the SNpc [14]. Therefore, it is understandable that microglia in the striatum and the SN displayed differential patterns of response to IT901 at 2 days after MPTP administration. Notably, mice in these two groups exhibited similar impairments in the behavioral tests, there may exist a “floor effect” in MPTP-induced injury to the striatal dopaminergic system.

Increased oxidative stress and chronic inflammation are involved in the initiation and progression of PD [1,3]. Further, oxidative stress and neuroinflammation have shown a reciprocal pattern of induction. The stimuli of oxidative stress and inflammation lead to the activation of NF-κB, and enzymes involved in the production of ROS and NO, and various inflammatory cytokines are targets of NF-κB. Changes in the levels of c-Rel and Rel-A are subsequent events after the treatment of MPTP/MPP^+ or LPS, however, alterations in c-Rel and Rel-A further modify the cellular oxidative stress and inflammation. Thus, activation of NF-κB, and oxidative stress and inflammation could play in a circuitry manner. In the brain of PD subjects, Rel-A expression is upregulated [11] and old *c-Rel* deficient mice display a spontaneous late-onset PD-like phenotype [12]. We found expression of NF-κB1 and Rel-A increased, whereas expression of c-Rel decreased in blood samples of PD patients. It is possible that increased oxidative stress and chronic inflammation decrease the levels of c-Rel, whereas they upregulate Rel-A expression. Hyperactivity of NF-κB pathway represented by Rel-A and NF-κB1 and hypoactivity of c-Rel might contribute to development and progression of PD.

In summary, c-Rel is neuroprotective in the progression of PD through pro-survival, anti-oxidative stress and anti-inflammation in neural cells (Fig. 7G). The imbalance in NF-κB activity is attributable to pathogenesis of Parkinson's disease.

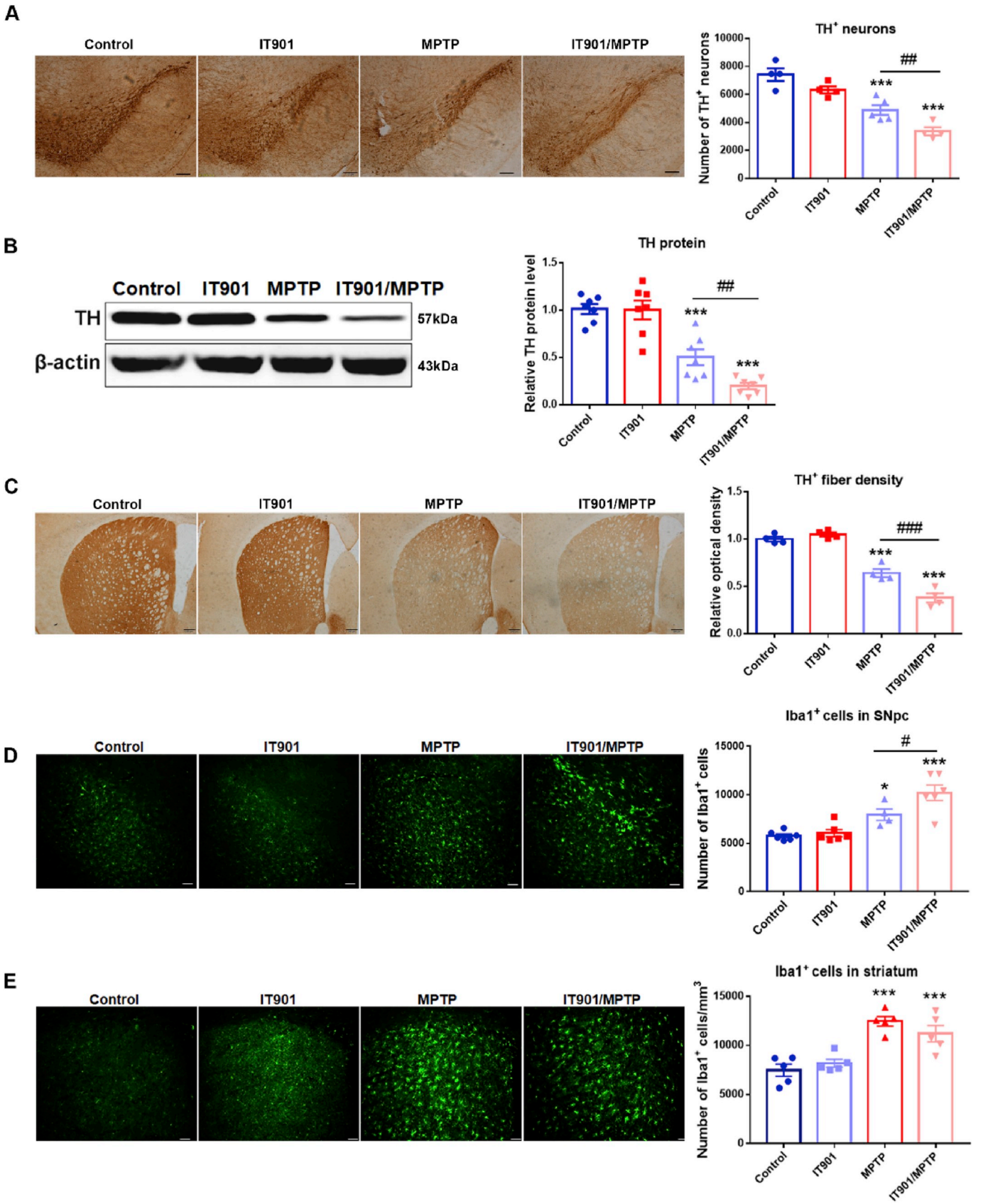

(caption on next page)

Fig. 7. IT901 aggravates MPTP-induced damages in the nigrostriatal pathway and the expression of NF-κB subunits in blood samples of control subjects and PD patients. (A) Immunohistochemical staining of TH in the substantia nigra at 2 days after saline or MPTP injection. Scale bar: 100 μm. Quantification of TH^+ neurons is shown in the right panel. n = 5–7. **(B)** Western blot analysis of TH expression in the striatum. D–S: DMSO-normal saline, I–S: IT901-normal saline, D–M: DMSO-MPTP and I–M: IT901-MPTP. Quantification of relative TH expression is shown in the right panel. n = 7. **(C)** Immunohistochemical staining of TH in the striatum. Scale bar: 100 μm. Densitometric analysis of TH staining is shown in the right panel. n = 5–7. **(D, E)** Immunofluorescence staining of Iba1 (green) in the substantia nigra **(D)** and the striatum **(E)** at 2 days after saline or MPTP administration. Scale bar: 50 μm. Stereological counting of $Iba1^+$ cells in the SNpc and quantification of $Iba1^+$ cells in the dorsal striatum are shown in the lower panel. n = 4–6. Differences were analyzed by one-way ANOVA followed by LSD multiple comparison tests. $^*p < 0.05$, $^{***}p < 0.001$, vs DMSO-normal saline groups; $\#p < 0.05$, $\#\#p < 0.01$, $\#\#\#p < 0.001$, vs DMSO-MPTP groups. **(F)** Transcripts of *Rel-A*, *c-Rel* and *NF-κB1* in blood samples of control subjects and PD patients, and ratios of c-Rel/Rel-A, c-Rel/NF-κB1 and Rel-A/NF-κB1. n = 27 for control subjects and n = 35 for PD patients. Data are expressed as the means ± SEM. Differences were analyzed by Mann Whitney test. $^*p < 0.05$, $^{**}p < 0.01$, $^{***}p < 0.001$, and $^{****}p < 0.0001$. **(G)** Diagram of the neuroprotection of NF-κB c-Rel subunit in PD models. (For interpretation of the references to color in this figure legend, the reader is referred to the Web version of this article.)

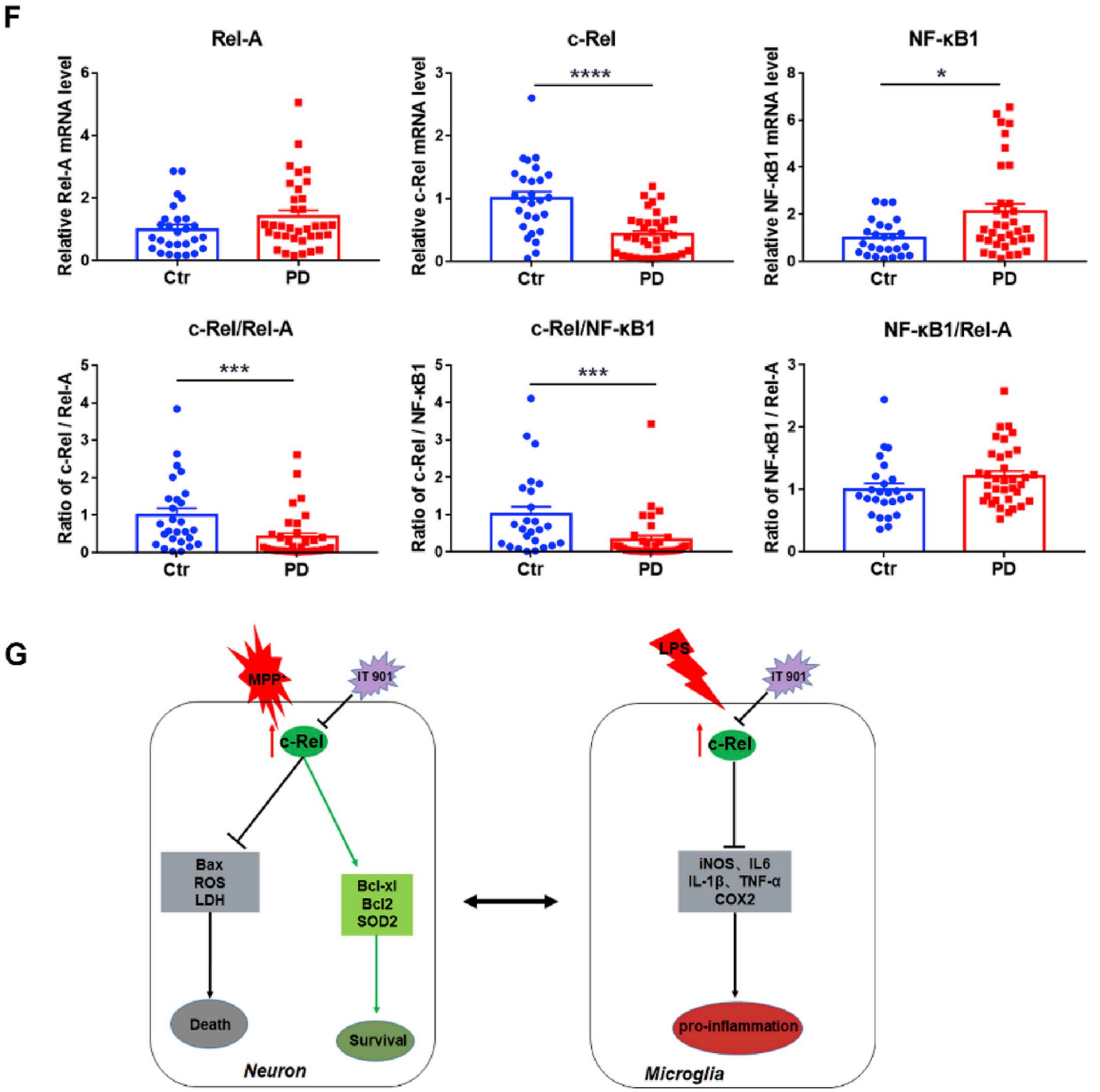

Fig. 7. (*continued*)

Author contributions

F.H., J.W., M.Y. and J.F. proposed and supervised the study. F.H., J.W., M.Y., Z.W. H.D. and J.W. wrote the manuscript. Y.T. contributed to the sample collection and clinical characterization of the patients. Z.W., H.D., J.W., Y.H., X.Z., Q.L., Y.M., J.T. and L.H. performed the experiments. Z.W., H.D., Y.H. and J.W. assisted in the preparation of the manuscript. All authors contributed to the interpretation of data and the revision of the manuscript.

Declaration of competing interest

The authors declare that they have no conflict of interest.

Acknowledgements

This work was supported by grants from the National Natural Science Foundation of China (31970908, 31671043 and 81571232) and Shanghai Municipal Science and Technology Major Project (No.2018SHZDZX01) and ZJLab. The authors are grateful to the study participants.

Appendix A. Supplementary data

Supplementary data to this article can be found online at https://doi.org/10.1016/j.redox.2020.101427.

References

[1] W. Dauer, S. Przedborski, Parkinson's disease: mechanisms and models, Neuron 39 (6) (2003) 889–909.
[2] M. Vila, S. Przedborski, Genetic clues to the pathogenesis of Parkinson's disease, Nat. Med. 10 (Suppl) (2004) S58–S62.
[3] C.K. Glass, et al., Mechanisms underlying inflammation in neurodegeneration, Cell 140 (6) (2010) 918–934.
[4] Q. Zhang, M.J. Lenardo, D. Baltimore, 30 Years of NF-kappaB: a blossoming of relevance to human pathobiology, Cell 168 (1–2) (2017) 37–57.
[5] A. Lanzillotta, et al., NF-kappaB in innate neuroprotection and age-related neurodegenerative diseases, Front. Neurol. 6 (2015) 98.
[6] R.H. Shih, C.Y. Wang, C.M. Yang, NF-kappaB signaling pathways in neurological inflammation: a mini Review, Front. Mol. Neurosci. 8 (2015) 77.
[7] J. Zeng, et al., TRIM9-Mediated resolution of neuroinflammation confers neuroprotection upon ischemic stroke in mice, Cell Rep. 27 (2) (2019) 549–560 e6.
[8] M. Srinivasan, et al., Nuclear factor-kappa B: glucocorticoid-induced leucine zipper interface analogs suppress pathology in an Alzheimer's disease model, Alzheimers Dement (N Y) 4 (2018) 488–498.
[9] L. Hou, et al., Inhibition of NADPH oxidase by apocynin prevents learning and memory deficits in a mouse Parkinson's disease model, Redox Biol. 22 (2019) 101134.
[10] A. Ghosh, et al., Selective inhibition of NF-kappaB activation prevents dopaminergic neuronal loss in a mouse model of Parkinson's disease, Proc. Natl. Acad. Sci. U. S. A. 104 (47) (2007) 18754–18759.
[11] S. Hunot, et al., Nuclear translocation of NF-kappaB is increased in dopaminergic neurons of patients with Parkinson disease, Proc. Natl. Acad. Sci. U. S. A. 94 (14) (1997) 7531–7536.
[12] C. Baiguera, et al., Late-onset Parkinsonism in NFkappaB/c-Rel-deficient mice, Brain 135 (Pt 9) (2012) 2750–2765.
[13] V. Porrini, et al., Mild inflammatory profile without gliosis in the c-rel deficient mouse modeling a late-onset parkinsonism, Front. Aging Neurosci. 9 (2017) 229.
[14] D. Huang, et al., Long-term changes in the nigrostriatal pathway in the MPTP mouse model of Parkinson's disease, Neuroscience 369 (2018) 303–313.
[15] H.L. Martin, et al., Evidence for a role of adaptive immune response in the disease pathogenesis of the MPTP mouse model of Parkinson's disease, Glia 64 (3) (2016) 386–395.
[16] X. Yang, et al., Functional imaging of Rel expression in inflammatory processes using bioluminescence imaging system in transgenic mice, PLoS One 8 (2) (2013) e57632.
[17] D.S. Cassarino, et al., The parkinsonian neurotoxin MPP+ opens the mitochondrial permeability transition pore and releases cytochrome c in isolated mitochondria via an oxidative mechanism, Biochim. Biophys. Acta 1453 (1) (1999) 49–62.
[18] Y. Shono, et al., Characterization of a c-rel inhibitor that mediates anticancer properties in hematologic malignancies by blocking NF-kappaB-Controlled oxidative stress responses, Cancer Res. 76 (2) (2016) 377–389.
[19] M. Pizzi, et al., Opposing roles for NF-kappa B/Rel factors p65 and c-Rel in the modulation of neuron survival elicited by glutamate and interleukin-1beta, J. Biol. Chem. 277 (23) (2002) 20717–20723.
[20] D. Schubert, H. Kimura, P. Maher, Growth factors and vitamin E modify neuronal glutamate toxicity, Proc. Natl. Acad. Sci. U. S. A. 89 (17) (1992) 8264–8267.
[21] C.W. Lu, T.Y. Lin, S.J. Wang, Quercetin inhibits depolarization-evoked glutamate release in nerve terminals from rat cerebral cortex, Neurotoxicology (Little Rock) 39 (2013) 1–9.
[22] P. Dohare, et al., The neuroprotective properties of the superoxide dismutase mimetic tempol correlate with its ability to reduce pathological glutamate release in a rodent model of stroke, Free Radic. Biol. Med. 77 (2014) 168–182.
[23] A. Sommer, et al., Th17 lymphocytes induce neuronal cell death in a human iPSC-based model of Parkinson's disease, Cell Stem Cell 23 (1) (2018) 123–131 e6.
[24] I. Sarnico, et al., NF-kappaB p50/RelA and c-Rel-containing dimers: opposite regulators of neuron vulnerability to ischaemia, J. Neurochem. 108 (2) (2009) 475–485.
[25] M. Pizzi, et al., NF-kappaB factor c-Rel mediates neuroprotection elicited by mGlu5 receptor agonists against amyloid beta-peptide toxicity, Cell Death Differ. 12 (7) (2005) 761–772.
[26] Y. Wang, et al., TLR4 participates in sympathetic hyperactivity Post-MI in the PVN by regulating NF-kappaB pathway and ROS production, Redox Biol. 24 (2019) 101186.
[27] S.D. Catz, J.L. Johnson, Transcriptional regulation of bcl-2 by nuclear factor kappa B and its significance in prostate cancer, Oncogene 20 (50) (2001) 7342–7351.
[28] T. Grimm, et al., EBV latent membrane protein-1 protects B cells from apoptosis by inhibition of BAX, Blood 105 (8) (2005) 3263–3269.
[29] J. Zhang, et al., ROS and ROS-mediated cellular signaling, Oxid. Med. Cell Longev. 2016 (2016) 4350965.
[30] C. Chen, L.C. Edelstein, C. Gelinas, The Rel/NF-kappaB family directly activates expression of the apoptosis inhibitor Bcl-x(L), Mol. Cell. Biol. 20 (8) (2000) 2687–2695.
[31] M. Idelchik, et al., Mitochondrial ROS control of cancer, Semin. Cancer Biol. 47 (2017) 57–66.